Initial results from an extreme ultraviolet interferometer operating with a compact laser plasma source

A. K. Ray-Chaudhuri,[a] K. D. Krenz, R. P. Nissen, and S. J. Haney
Advanced Electronic Manufacturing Dept., Sandia National Laboratories, Livermore, California 94550-0969

C. H. Fields
Department of Electrical Engineering and Computer Science, University of California-Berkeley, California 94720

W. C. Sweatt
Optics and Exploratory Technologies Department, Sandia National Laboratories, Albuquerque, New Mexico 87185

A. A. MacDowell
Lucent Technologies, Bell Laboratories, 510E Brookhaven Lab, Upton, New York 11973

When characterizing an extreme ultraviolet (EUV) lithographic optical system, visible light interferometry is limited to measuring wave front aberration caused by surface figure error while failing to measure wave front errors induced by the multilayer coatings. This necessitates the development of interferometric techniques at an EUV camera's operational wavelength (at-wavelength testing), which is typically around 13 nm. While a laser plasma source (LPS) is being developed as a lithography production source, it has generally been considered that only an undulator located at a synchrotron facility can provide the necessary laserlike point source brightness for EUV interferometry. Although an undulator-based approach has been successfully demonstrated, it would be advantageous to test a camera in its operational configuration with an LPS. We are developing the latter approach by utilizing extended source size schemes to provide usable flux throughput. A slit mounted at the source plane can provide the necessary spatial coherence for lateral shearing interferometry. Initial results from an EUV lateral shear interferometer based on the Ronchi test are presented. © *1996 American Vacuum Society.*

I. INTRODUCTION

Extreme ultraviolet lithography (EUVL) is a candidate technology for the microelectronics industry with design rules for 0.1 μm features and below.[1,2] The basic concept of EUVL is to utilize near-normal incidence multilayer-coated reflective aspheric optics operating at a typical wavelength of $\lambda_{EUV} = 13$ nm. A major challenge for this technology is the fabrication of optical systems with unprecedented requirements for wave front aberration control. A fundamental limitation of visible light techniques is that they can only measure the *surface* wave front error generated by an optical system, whereas a multilayer-coated optical system has effects that depend on the buried interfaces. Because the reflectivity and phase shift upon reflection from a multilayer coating vary with the incident angle and layer spacing, a departure from either the ideal figure or multilayer coating specification can induce unwanted apodization as well as wave front error.[3] These theoretical effects can be readily calculated.[4] Thus, the final alignment and qualification of an EUV camera will have to be performed at the functional wavelength of the optical system under test (''at-wavelength''.[5])

II. EXPERIMENTAL APPROACH

In visible light interferometry, a high brightness (photons/unit solid angle/unit source area) laser illuminating a pinhole provides a point source that is both spatially and temporally coherent. Analogously, several research groups have utilized an undulator located at a synchrotron facility to provide a bright point source for EUV interferometry.[6–8] Although such an approach has been successful, the high cost and the limited availability of an undulator are impediments to widespread use by an optics manufacturer or an end user. It is necessary for EUV interferometry to evolve into an in-house technique.

Our approach to this problem is to realize that one can select a metrology technique which can utilize a slit source and still provide the necessary spatial coherence requirements of the technique. In this way, one can increase the delivered coherent flux (photons/s) by several orders of magnitude. This allows more compact and less expensive sources to be utilized despite the lowered source brightness.

A. Extended source lateral shearing interferometry

Two points on a wave front located at the optic's pupil plane, emanating from a source a distance f away, are considered to have a high degree of mutual coherence if they are capable of producing high contrast interference fringes. For a pinhole source, this condition is satisfied by two points on the wave front oriented in any lateral direction. As their lateral separation increases, the interference contrast decreases. For a slit source, high contrast interference fringes are lim-

ited to two points on a wave front oriented in one lateral dimension. In order to obtain two-dimensional wave front information, two separate measurements are obtained with orthogonal slit sources. A slit source can be utilized in the classic Ronchi test, which can be considered to be multiple-beam lateral shearing interferometry (LSI).[9] In this technique, a transmission diffraction grating is positioned near the image plane. The grating period is selected such that the lateral shear between adjacent orders is small. Multiple-beam interference occurs in the region of overlap. For a quasi-monochromatic source illumination, the zero-order beam and the $\pm$ first-order beams are much more intense and can be considered to be the only sources of interference. For low values of shear, the various modes of interference overlap each other and a two-beam interference model can be utilized.

In LSI, two interfering wave fronts sheared in the x direction yield the phase difference

$$\phi_x(x,y) = W_x(x,y) - W_x(x-s,y). \tag{1}$$

The term $\phi_x(x,y)$ is the difference in the phases of the wave fronts at the two points (x,y) and $(x-s,y)$. For a wavelength λ, grating period d, and distance between the grating and the interference observation plane L_1, the lateral shear (s) in the observation plane is given by

$$s = \left(\frac{\lambda}{d}\right)L_1. \tag{2}$$

As the shear approaches zero, the wave front can be related to the phase difference by the equation

$$\frac{dW_x(x,y)}{dx} = \frac{\phi_x(x,y)}{s}. \tag{3}$$

Thus, for small values of shear, LSI is a direct measure of the wave front derivative in the direction of the shear. To obtain a two-dimensional wave front map, shearing measurements must also be performed in the orthogonal direction to obtain $W_y(x,y)$ and combined together with $W_x(x,y)$. The sensitivity of this technique at EUV wavelengths has been measured by Bjorkholm *et al.* and found to be better than 0.021 waves rms, thus validating this model.[7]

EUV lateral shearing interferometry has the practical advantage of a large dynamic operational range. This can be obtained by using rulings of different pitch. This property is extremely important for enabling mechanical designs with *in situ* adjustments that can utilize an at-wavelength technique for the complete alignment. As the alignment is improved, a higher frequency ruling provides higher sensitivity. An additional advantage of this technique is the common path design; no EUV reference optics are required to test the optical system.

B. Source spatial coherence requirements

There is a significant advantage in utilizing LSI with small shear in that the source spatial coherence requirements are not stringent, thus enabling the use of larger source sizes. For interferometric techniques which require full spatial co-

herence across the width (D) of the illuminated optic under test, the source width should be $(\lambda/D)f$. For LSI, the spatial coherence need only be sufficient such that interference can be observed (i.e., full spatial coherence exists) between two points of the wave front separated by the *shear distance*. Thus, the source width can be $(\lambda/D)f(D/s) = (\lambda/S)f$, which affords a much larger source.[10] This advantage is extremely useful when trying to illuminate a larger numerical aperture system with sufficient flux.

C. Phase-shifted analysis

Phase-shifting analysis has been previously combined with LSI. [10,11] By laterally translating the grating in the shear direction, a phase shift is imparted to the interference pattern which is recorded by a charge coupled device (CCD) camera. The advantages of phase shifted interferometry (PSI) include increased resolution and insensitivity to factors such as spatial variation in intensity, detector sensitivity, and fixed pattern noise. For these initial experiments, a "three-step" algorithm was selected for its simplicity.[12] Three interferograms, each separated by $\pi/2$ phase shift $(0, \pm \pi/2)$ are acquired. The phase difference is given by

$$\phi_x(x,y) = \tan^{-1}\left(\frac{I_1 - I_3}{2I_2 - I_1 - I_3}\right), \tag{4}$$

where I_1, I_2, and I_3 are the fringe intensities recorded at pixel (x,y) for phase shifts of $\pi/2, 0$ and $+\pi/2$, respectively. Since a $\tan^{-1}$ calculation limits the value of ϕ_x from $-\pi$ to $+\pi$, phase profile discontinuities will have to be removed. Finally, the periodic 2π phase discontinuity is removed.

In an EUV optical system a mirror surface imperfection can lead to substantially decreased reflectance at specific points on the pupil. The wave front from such areas cannot be measured with any degree of certainty. Thus it is important to calculate, as a figure of merit, the data modulation
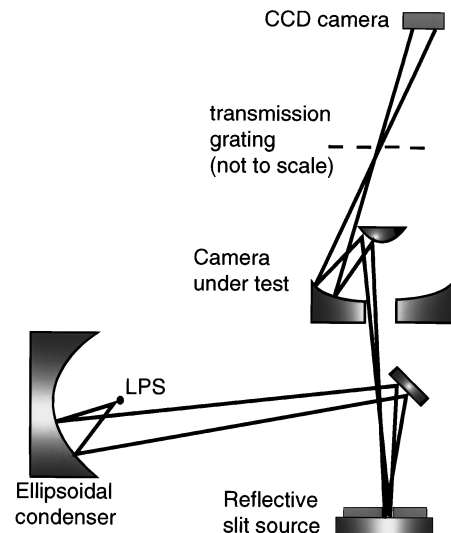

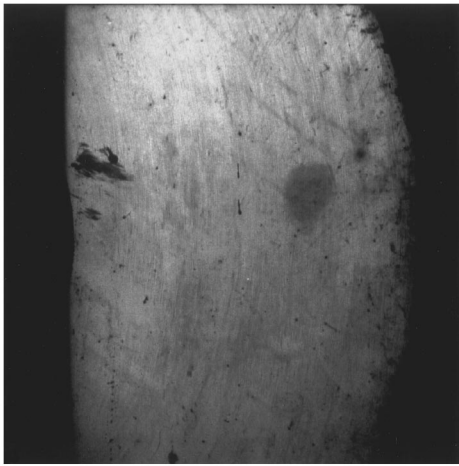FIG. 1. Schematic diagram of experimental setup utilized for EUV interferometry.

FIG. 2. Far field EUV image of Schwarzschild camera as illuminated in Fig. 1 without a transmission grating. One can note both defect areas and sub-mm roughness due to coarse polishing.

(γ_x) which is defined as the ratio of intensity modulation to average intensity at each pixel. For the three-step algorithm, γ_x is given by

$$\gamma_x(x,y) = \frac{[(I_1 - I_3)^2 + (2I_2 - I_1 - I_3)^2]^{1/2}}{I_1 + I_3}.\qquad(5)$$

Pixels with a decreased γ_x are masked during the calculation of the three-step algorithm.

III. EXPERIMENTAL SETUP

Figure 1 is a schematic of the interferometer setup installed on a five multilayer mirror, laboratory EUV exposure system located at Sandia National Labs in Livermore, CA.[13] All multilayer mirrors are optimized for peak EUV reflectance at a wavelength of 13.4 nm. A Nd:YAG (1.06 mm) laser capable of 800 mJ, 9 ns pulses at a 20 HZ repetition rate is focused on a metal target. The extremely hot plasma
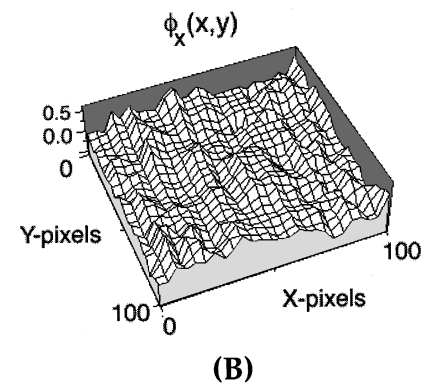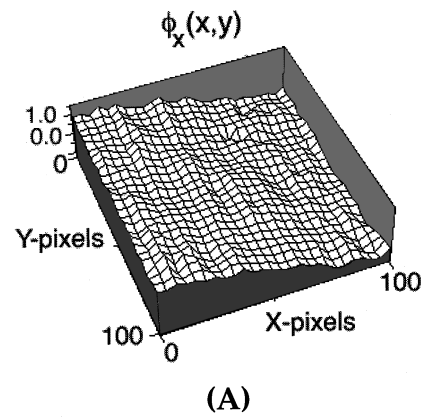

(A)

(B)

FIG. 4. The phase difference $\phi_x(x,y)$ before (a) and (b) subtracting out the defocus term. Each pixel is 25 μm$\times$25 μm in the observation plane. Sub-mm roughness is quite pronounced after defocus is removed.

that is created has a continuous radiation spectrum that extends into the EUV regime. An ellipsoidal condenser mirror magnifies the source by 13.3 times and projects the image to the reflective mask object plane. The entrance pupil of a 10$\times$ reduction Schwarzschild camera is located off axis to avoid the central obscuration. Under normal operation, the con-
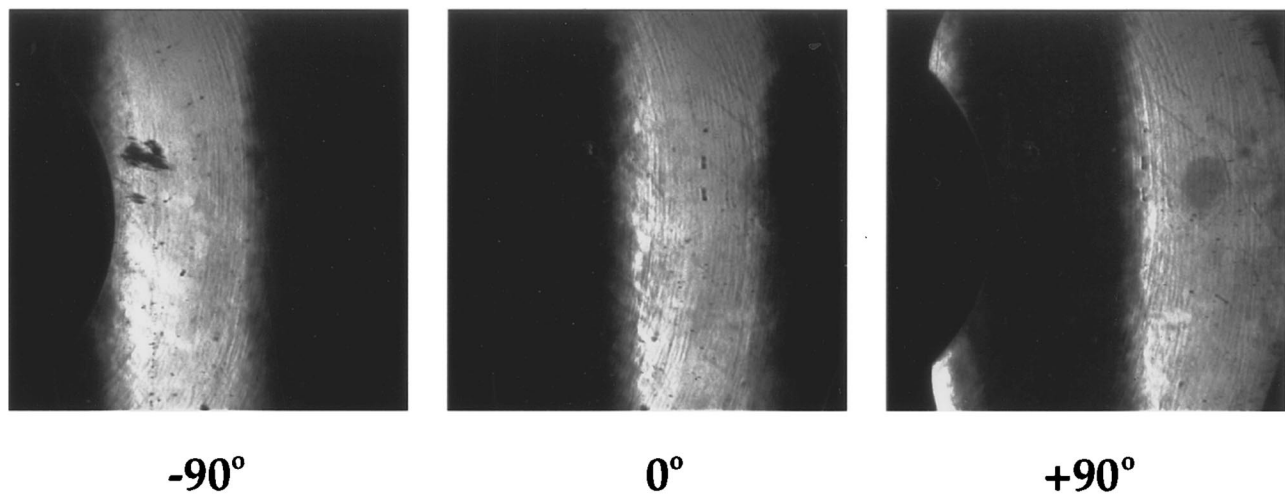

-90°   **0°**   **+90°**

FIG. 3. A series of phase-shifted interferograms obtained with a 20 μm period grating placed 130 μm from focus. The grating was laterally translated 5.0 μm between each interferogram.
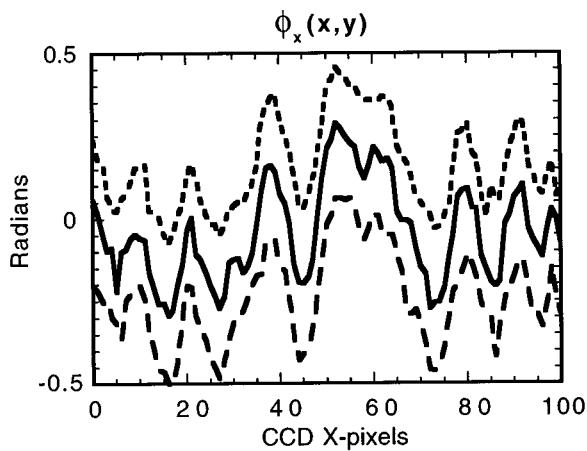
FIG. 5. Adjacent lineouts along the x axis from the center of the aperture. The adjacent features are high correlated. From the finer structure, a derivative sensitivity less than 0.2 rad is estimated.

denser is adjusted to focus the source image on the pupil plane to produce a pupil fill factor of approximately 0.5.

A turning mirror deflects the condenser illumination on to a reflective multilayer mask. The camera's well-corrected field size is 0.4 mm in diameter. For these initial experiments, sufficient coherent flux was obtained with a 25-μm-wide slit source defined at the reflective mask image plane. The source length was approximately 1.5 mm to match the camera's well-corrected field of view. Diffraction gratings for insertion near the image plane were defined by laser-drilling copper foil.

To enable alignment, the reflective mask is mounted on a vacuum compatible, x-y-z-θ crossed roller bearing stage. The diffraction grating is mounted on an x-y stage of similar design. An EUV solid state photodiode measured the transmitted contrast signal as the grating is scanned and brought into θ alignment with the slit source. For the fine translation during phase shifting analysis, a piezoelectric stack with capacitive position feedback translated the ruling. The position feedback, accurate to 1 nm, ensured that any translation error was minimized.

The EUV detector is a Peltier-cooled CCD camera containing a 1024×1024 pixel, back-illuminated CCD. Each pixel is 25×25 μm in size and has a dynamic range of 15 bits. A 1 μm Be membrane is utilized as an EUV high pass filter to block unwanted radiation on the CCD. The transmission at 13.4 nm is approximately 20% for this filter.

IV. EXPERIMENTAL RESULTS

Figure 2 is an EUV image acquired by the camera when positioned in the far field of the Schwarzschild camera at a distance of 75 mm from the image plane with no transmission ruling in place. The recording duration for this low noise image was 1 min. In addition to observing what appears to be digs in the mirror substrate which sharply decrease reflectance, there are subtle reflectance variations which show a scoring of the entire surface in the radially
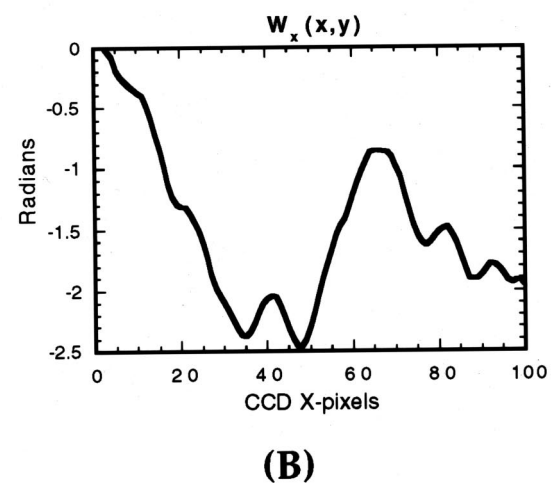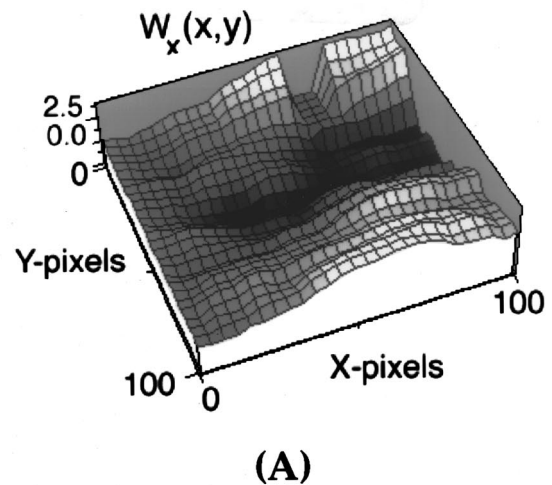

(A)

(B)

FIG. 6. (a) The wave front displacement in the x direction. A rms value of 0.25 waves is measured. (b) A lineout is taken along the x axis in the center of the aperture. High frequency features are discernable, but relatively low frequency figure errors dominate.

tangent direction. These features are sub mm in dimension and were only observable with slit source illumination which had a sufficient degree of spatial and temporal coherence. The origin of these features may be attributed to the initial coarse polishing of the mirror substrates. Since these features were not observed with visible light interferometry during the fabrication process, they were not removed with subsequent polishings. Such information may help in improving the fabrication process.

To investigate the nature of the observed microroughness, LSI was performed. Figure 3 shows three lateral shearing interferograms obtained with a 20 μm period diffraction grating placed 130 μm from the image plane. At this grating position in the optical axis, only one fringe is observed. The grating was translated 5.0 μm between the acquisition of each interferogram. Compared to Fig. 2, the previously observed microroughness features now have increased contrast; as is expected for phase imaging. The value of $\theta_x(x,y)$ was computed using this data with the three-step algorithm. Spe-

cialized software was written to take advantage of the CCD dynamic range rather than use commercial software which is limited to 8 bits. A sub-aperture corresponding to a numerical aperture of ~0.03 on the image side is plotted in Fig. 4(a). The observed linear dependence for ϕ_x is directly related to the defocus of the grating. A low reflectance, substrate defect area has been masked during the analysis. The defocus term is removed and the results are plotted in Fig. 4(b). The striations due to the coarse polishing are again clearly evident. Figure 5 shows a plot of an adjacent set of lineouts along the x axis taken at the center of the sub-aperture. Specific fine structure features which are common to these adjacent rows are on the order of 0.2 rad, signifying a high degree of measurement sensitivity. From Eq. (2), the value of s is 50 μm in our experimental setup. Figure 6(a) shows the plot of $W_x(x,y)$ after following the calculation of Eq. (3). The relatively low frequency features are now more evident. A lineout along the x axis is taken at the center of the sub-aperture [Fig. 6(b)]. The wave front rms value across the sub-aperture is 1.60 rad (0.25 waves).

V. SUMMARY

A method for performing EUV interferometry with a laser plasma source has been implemented. To make use of the relatively low brightness of a laser plasma source, extended source lateral shearing interferometry based on the Ronchi technique was selected. This will enable the in-house alignment of an EUV lithographic optical system by making EUV interferometry more readily available to both the optical manufacturer as well as the end user. Initial one-dimensional results from a sub-aperture of a Schwarzschild camera indi-

cate that this technique can detect the wave front difference of sub-mm spatial features with a sensitivity better than 0.2 rad (0.03 waves). Future work will address remaining issues regarding the precision required for fabricating diffraction gratings, what values of shear are practical to use, and quantifying the accuracy of this technique.

[1] J. E. Bjorkholm *et al.*, J. Vac. Sci. Technol. B **8**, 1509 (1990).
[2] D. A. Tichenor *et al.*, Appl. Opt. **32**, 7068 (1993).
[3] B. Lai, F. Cerrina, and J. H. Underwood, in *Applications of Thin-Film Multilayered Structures to Figured X-ray Optics*, Proc. SPIE, Vol. 563, p. 174.
[4] J. H. Underwood and T. W. Barbee, Appl. Opt. **20**, 3027 (1981).
[5] D. Attwood, G. Sommargren, R. Beguiristain, K. Nguyen, J. Bokor, N. Ceglio, K. Jackson, M. Koike, and J. Underwood, Appl. Opt. **32**, 7022 (1993).
[6] A. K. Ray-Chaudhuri, W. Ng, F. Cerrina, Z. Tan, J. Bjorkholm, D. Tennant, and S. J. Spector, J. Vac. Sci. Technol. B **13**, 3089 (1995).
[7] J. E. Bjorkholm, A. A. MacDowell, O. R. Wood II, Z. Tan, B. LaFontaine, and D. M. Tennant, J. Vac. Sci. Technol. B **13**, 2919 (1995).
[8] K. A. Goldberg, R. Beguiristain, J. Bokor, H. Medecki, D. T. Attwood, K. Jackson, E. Tejnil, and G. E. Sommargren, J. Vac. Sci. Technol. B **13**, 2923 (1995).
[9] A. Cornejo-Rodriguez, in *Optical Shop Testing*, edited by D. Malacara (Wiley, New York, 1992), pp. 321–365.
[10] T. Yatagai, Appl. Opt. **23**, 3676 (1984).
[11] K. Omura and T. Yatagai, Appl. Opt. **27**, 523 (1988).
[12] K. Creath, in *Progress in Optics*, edited by E. Wolf (Elsevier, Amsterdam, 1988), Vol. XXVI, pp. 349–393.
[13] D. A. Tichenor *et al.*, Proc. SPIE **2194**, 95 (1994).